J. Fluid Mech. (1987), *vol.* 180, *pp.* 429–449
Printed in Great Britain

On the motion of linearly stratified rotating fluids past capes

By DON L. BOYER AND LIJUN TAO†
Department of Mechanical Engineering, University of Wyoming, Laramie, WY 82071, USA

(Received 29 July 1986 and in revised form 10 December 1986)

This is an experimental investigation of the flow of an impulsively started linearly stratified, rotating fluid past obstacles located on either the right or left side of a channel of rectangular cross-section. The obstacle has plane sloping sides so as to represent a cape-like feature extending from a shoreline. Emphasis is given to the temporal flow development in the lee of the obstacle. The pertinent dimensionless parameters are the Rossby, Burger and Ekman numbers, the ratio of the fluid depth to obstacle width and the obstacle-to-channel-width ratio.

For sufficiently small Burger numbers and for a range of Rossby numbers the right-side obstacle produces fully attached flows at all levels. At larger Burger numbers attached lee anticyclones develop during a period of the order of ten advective timescales. At still larger Burger numbers the starting lee anticyclone is shed and followed by a weaker secondary anticyclone.

No fully attached regime could be found for the left-side obstacle for the range of parameters considered. For the smallest Burger numbers studied and for a range of Rossby numbers, a lee cyclone is formed on the order of one advective timescale; this eddy spins down at large times leaving a quiescent wake. At larger Burger numbers and for a range of Rossby numbers, cyclonic eddy shedding occurs.

Measurements of the streamwise location of the eddy centres, the streamwise extent of the eddies and the vorticities of the eddy cores are made as functions of a dimensionless time and the system parameters. It is found, for example, that the vorticity of the starting eddies at small times in the eddy-shedding regimes for both anticyclones and cyclones is strongest at the lowest observation levels. Ekman suction, however, tends to more strongly decrease the vortex strength in the lower levels compared to the middle levels so that at large times the vorticity in the middle levels exceeds that near the channel floor. Eddies with similar characteristics are found in the open ocean.

1. Introduction

Beginning with the work of Davies (1972) there has been an increasing emphasis on the laboratory investigation of the combined effects of stratification and background rotation on flow past topographic features. Davies considered the motion past an isolated sphere at a fixed Rossby number of 4.4×10^{-3} and a fixed Ekman number of 1.0×10^{-4}, both based on the sphere diameter; he then investigated the flow behaviour in the vicinity of the sphere for a range of a stratification parameter defined as the ratio of the Brunt-Väisälä frequency to the Coriolis parameter. Davies showed that as stratification is increased, background rotation being fixed, the strength of

† Visiting Scientist from the Institute of Atmospheric Physics, Academia Sinica, Beijing, China.

the Taylor column at a given height above the sphere is weakened; i.e. more fluid tends to pass through an imaginary vertical cylinder circumscribing the sphere. An excellent review article on laboratory experiments on topographic effects on rotating and/or stratified flows has been given by Baines & Davies (1980).

More recently one of us has conducted a laboratory study of the wake region behind an obstacle in a rotating and stratified flow; see Boyer *et al.* (1987). This investigation is for Rossby numbers one to two orders of magnitude larger than that considered by Davies (1972). As such the wake region for the larger-Rossby-number experiments is associated with eddy formation and shedding. The study by Boyer *et al.* (1987) also discusses the effect of rotation on the formation of lee waves and shows how a quasi-geostrophic numerical model can be used to predict streamline deflections at various levels for cases in which the Rossby number is small enough that eddy formation and shedding does not occur.

In the present study we consider the flow of a linearly stratified fluid past obstacles located on either the right or left sides (facing downstream) of a rotating channel; the physical system is given schematically in figure 1. The obstacle, as indicated, has sloping sides and the motion relative to the topography is established by translating the channel floor, to which the obstacle is fixed, at a constant speed U in the negative x-direction. The channel height H, width L, and horizontal obstacle dimension D, characterize the geometry. Note that only a single obstacle shape is considered so that H and D are sufficient to specify the geometry. The rotation is anticlockwise and is characterized by the frequency $\omega = \frac{1}{2}f$. The stratification is characterized by a constant Brunt–Väisälä frequency $N = (g\Delta\rho_s/H\rho_s)^{\frac{1}{2}}$, where g is the acceleration due to gravity, $\Delta\rho_s$ is the density difference between the channel floor and the rigid horizontal lid confining the fluid from above, and ρ_s is the mean density.

It is a straightforward matter to show that the flow characteristics for this system depend on the Rossby, $Ro = U/fD$, Ekman, $E = \nu/fH^2$, and Burger, $S = N^2H^2/f^2D^2$, numbers as well as the geometric parameters H/D and D/L, where ν is the kinematic viscosity. Note that a Reynolds number, $Re = UD/\nu$, can also be defined but is not independent of the above because $Re = (Ro/E)(D^2/H^2)$; i.e. only two of Ro, E and Re are independent.

The study of such a physical system is motivated by possible applications to the flow of ocean currents past capes and/or island topographies. For the obstacle on the right, eddying motion in the lee has the tendency to develop anticyclonic relative vorticity for the northern hemisphere or vertically upward rotation as indicated in figure 1; for the obstacle on the left, the tendency is for cyclonic vorticity in the lee.

While the present work is not directed at any particular oceanographic situation it is in order to note some estimates of the various dimensionless parameters for a typical one. To this end, with primes denoting oceanographic parameters, we take $H' \approx 1.0$ km, $D' \approx 50$ km, f' (mid-latitudes) $\approx 10^{-4}$ s^{-1}, $N' \approx 3 \times 10^{-3}$ s^{-1}, $U' \approx 10$ cm s^{-1} and $1 < \nu_V' < 10^3$ cm^2 s^{-1}, where ν_V' is a vertical eddy viscosity (see Pedlosky 1979). These values lead to $Ro \approx 0.02$, $S \approx 0.36$, $10^{-6} < E_V < 10^{-3}$ and $H/D = 0.02$. With the exception of the obstacle aspect ratio H/D, which is much smaller in the ocean than in the laboratory, these various oceanographic dynamical quantities can be matched in the laboratory.

As discussed in Pedlosky (1979) and shown in some detail in a recent paper by one of the present authors, Boyer & Biolley (1986), similarity of the quasi-geostrophic potential-vorticity equation for the oceans and for a laboratory system such as discussed herein, does not require the matching of the obstacle aspect ratio D/H since that parameter appears only in the expression for the Burger number; i.e. it does not

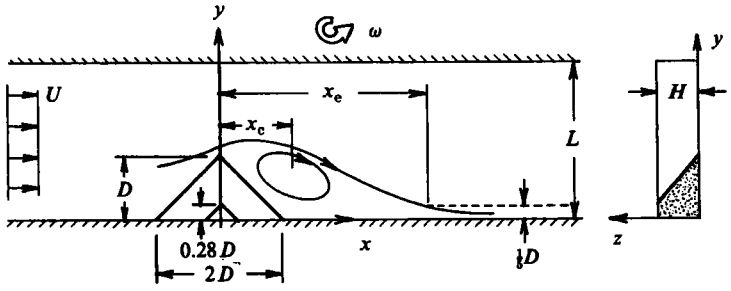

FIGURE 1. The physical system.

appear separately in the lowest-order equations of motion or boundary conditions. Strict geometric scaling is hence not required in the laboratory modelling, similarity requiring only that Ro, E and S be matched. In summary, while oceanic modelling is not the principal focus herein, that line of investigation looks promising because the present laboratory system can replicate the most important dimensionless parameters. Such additional complexities as non-constant Brunt–Väisälä frequencies, could also be introduced.

In a recent study, Griffiths & Linden (1983, hereinafter referred to as GL), conducted a series of laboratory experiments on a similar physical system, but restricted to homogeneous incompressible flows. In particular they considered the flow past truncated and full (i.e. extending throughout the fluid depth) semi-circular cylinders as well as quarter spheres. For the truncated cylinders and quarter spheres and the obstacles on the right wall, GL found that for sufficiently small Rossby numbers an approximate Taylor column formed above the topography and the free-stream fluid moved past the obstacle and vertical circumscribing cylinder in approximately a two-dimensional pattern; there was little influence on the motion several characteristic horizontal dimensions downstream of the topography. At larger and larger Rossby numbers more and more fluid was observed to pass over the crest of the topographic features.

For the obstacle mounted on the left, however, the topography had a large downstream influence for all parameters investigated. For the lowest-Rossby-number experiments (i.e. $Ro \approx 0.01$) the flow was found to be blocked at all levels (i.e. above and below the top of the obstacle) with the fluid separating from the obstacle and imaginary circumscribing cylinder; the blocked region in certain cases was found to be wider than the obstacle itself and to extend far downstream, sometimes encompassing the entire length of the channel. At larger Ro for the left-side obstacle the wake flow became unstable with cyclonic eddies formed which were then advected downstream with the mean flow.

While stratification, as considered herein, substantially modifies the dynamics of the physical system, some of our observations are reminiscent of the GL experiments and these similarities (and differences) will be discussed below. The present study is primarily an observational one in the sense that the authors do not address an accompanying analytical or numerical model. We do attempt to give a detailed description of the resulting flow field, both qualitatively and quantitatively, so that the results can be used to compare with future analytical or numerical models.

The focus in the experiments is on the temporal development of the velocity field as the obstacle is given an impulsive velocity U at the initiation of the experiment. While for certain regions of parameter space the flow field reaches an approximate

$0.15 \leqslant U \leqslant 1.5$ cm s^{-1}	$D = 13$ cm
$0.1 \leqslant \omega \leqslant 0.5$ s^{-1}	$\nu = 0.01$ cm^2 s^{-1}
$H = 8.1$ cm	$0.30 < N < 1.1$ s^{-1}

TABLE 1. Experimental parameters

steady state prior to the completion of the obstacle traverse through the channel, in others the flow field is clearly continuing to develop. It is important to keep in mind this developing nature of the flow as one interprets the results.

In §2 we briefly discuss the experimental apparatus and the various observational techniques employed. In §3 a qualitative description of the various characteristic flow patterns is presented. Emphasis is given to the differences between flows for right- and left-side features and to variations of the flow patterns with depth. Flow-regime diagrams of Burger against Rossby number are presented which depict the regions of parameter space for which the various characteristic flow patterns can be observed. In §4 quantitative measures of the various flows are presented. Measures of the streamwise location and extent of the eddying motion in the lee are defined and these are used as one observable for the temporal development of the motion and its approach to steady state. Measurements of the evolution of vorticity in the eddy core as a function of the various system parameters are also presented. Finally a summary of some of the most important observations is given in §5.

2. Experimental apparatus and techniques

The apparatus used for the present experiments, was discussed in some detail in a previous communication; see Boyer & Kmetz (1983). The facility is a rotating tow tank 2.4 m long, 43 cm wide and 30 cm deep. Topographic features are mounted on a flexible belt located on the channel bottom which in turn can be translated at a constant speed in the range $0.1 \leqslant U \leqslant 4.0$ cm s^{-1} along the channel axis. The tank is filled whilst at rest with a salt stratified water solution using the now classic Oster (1965) technique. The fluid is confined from above by a rigid horizontal Plexiglas lid. After the tank is filled the desired rotation rate is achieved by increasing the rotation in small increments over a period of 20–30 min; this allows one to maintain a specified vertical density gradient. The range of rotations utilized was $0.10 < \omega < 0.50$ s^{-1} with the upper limit required so as to ensure that centrifugal effects were negligible.

Neutrally buoyant polystyrene particles of diameter 0.5 mm are embedded in the fluid for flow visualization. The facility is equipped with a tow carriage which moves synchronously with the belt. A light source, providing a horizontal sheet of illumination of thickness 0.5–1.0 cm, together with a 35 mm camera are mounted on the carriage. The approximate horizontal Eulerian velocity field and associated streamlines can thus be determined using particle-streak photography. For some experimental runs the observation level was continually being changed between three different levels. The advantage of this method was that the time development of the flow could be investigated at various levels during the same experiment. A disadvantage was that simultaneous observations at different levels were not realized. The experimental parameters considered are delineated in table 1.

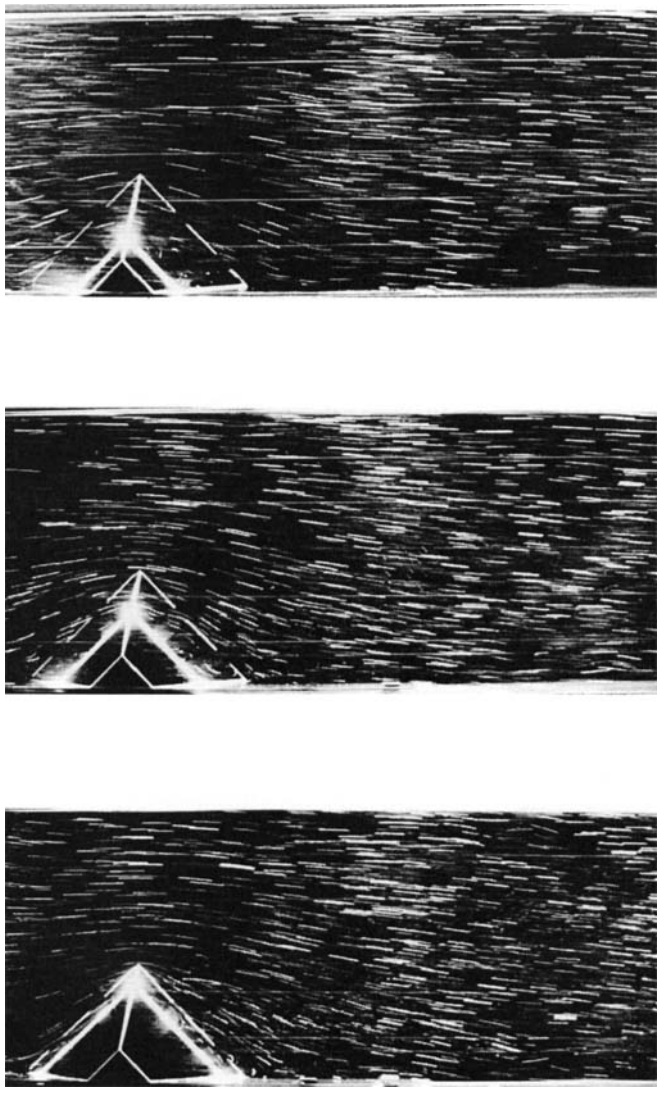

FIGURE 2. Vertical structure for right-side obstacle in the fully attached-flow regime; $Ro = 0.058$, $S = 0.15$, $E = 1.6 \times 10^{-4}$ ($Re = 990$); (*a*) $r^* = 9.6$, $z^* = 0.75$, (*b*) 9.6, 0.50, and (*c*) 9.8, 0.25.

3. Experimental results – qualitative

The initial experiments were addressed to determining the general character of the flow field for both left- and right-side obstacles for the range of parameters indicated in table 1 and for various elevations. The observation levels chosen were $z^* = z/H = 0.25$ (low), $z^* = 0.50$ (middle) and $z^* = 0.75$ (high). The lowest level was typically at from 7–14 δ_E above the bottom Ekman layer where $\delta_E \sim (\nu/\omega)^{\frac{1}{2}}$ is the Ekman layer thickness.

For sufficiently small S and for a range of Rossby numbers for the right obstacle, the horizontal flow pattern was observed to be fully attached for all observation times and at all levels. Flow patterns at the high, middle and lower levels near the end of the traverse are given, respectively, in figure 2 (*a–c*). The bright triangular streak on

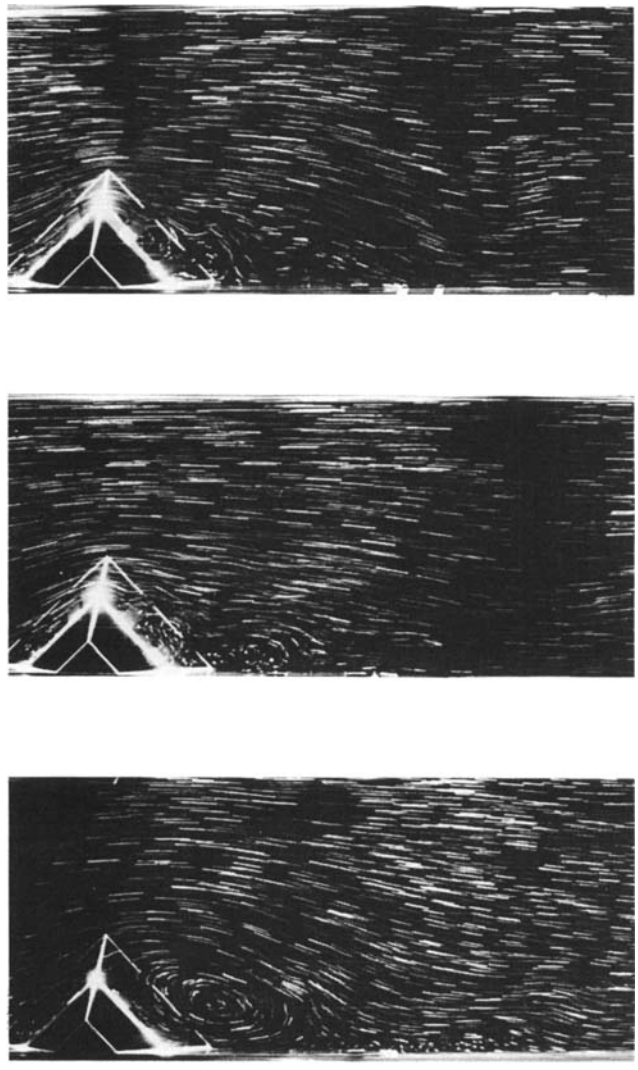

FIGURE 3. Temporal development of attached-anticyclonic-eddy regime; $Ro = 0.058$, $S = 0.31$, $E = 1.6 \times 10^{-4}$ ($Re = 990$), $z^* = 0.50$; (*a*) $\tau^* = 3.8$, (*b*) 7.3 and (*c*) 10.6.

the obstacle is a reflection of the horizontal light beam used to illuminate the polystyrene particles; its location on the obstacle indicates the observation level of the respective photographs. The flow on this and succeeding photographs is from left to right with the rotation being vertically upward. The dimensionless times $\tau^* = Ut/D$ given in the captions of figure 2 (*a–c*) and succeeding illustrations indicate the time from the impulsive start of the obstacle motion; t is the dimensional time. For the typical oceanic values given above, $\tau^* \approx 1$ corresponds to 5–6 days.

Note the fore-and-aft symmetry at all levels in figure 2 (*a–c*). We recall that the GL observations for a homogeneous fluid at low Rossby numbers for a right-side obstacle produced a Taylor-column effect above the topography. Davies (1972), in his isolated-topography experiments also noted a Taylor-column effect. In the stratified case of figure 2 such a column is not present, the fluid motion near the

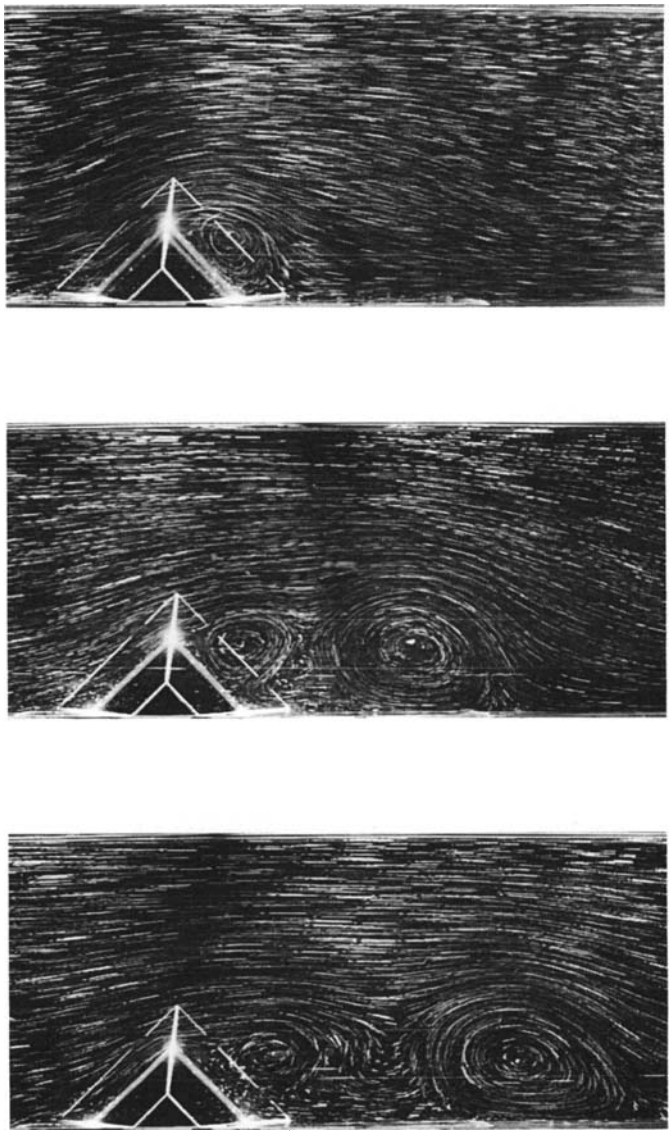

FIGURE 4. Temporal development of anticyclonic-eddy-shedding regime; $Ro = 0.13$, $S = 6.48$, $E = 6.2 \times 10^{-4}$ ($Re = 550$), $z^* = 0.50$; (*a*) $\tau^* = 1.0$, (*b*) 5.0 and (*c*) 8.9.

obstacle being approximately tangent to the topography surface at all levels. The Rossby number is an order of magnitude larger than that for the Davies experiments and substantially larger than that for the lowest-*Ro* GL experiments; it is for this reason that a Taylor-column effect in this and succeeding experiments is not observed in the present studies.

We recall, also, that GL noted only small disturbances in the near wake and this is again noted for the obstacle on the right in the stratified case at sufficiently small *S*. The flow patterns in figure 2 seem to have reached an approximately steady state by the end of the obstacle traverse. We term the flow-pattern characteristics of figure 2 as 'fully-attached'.

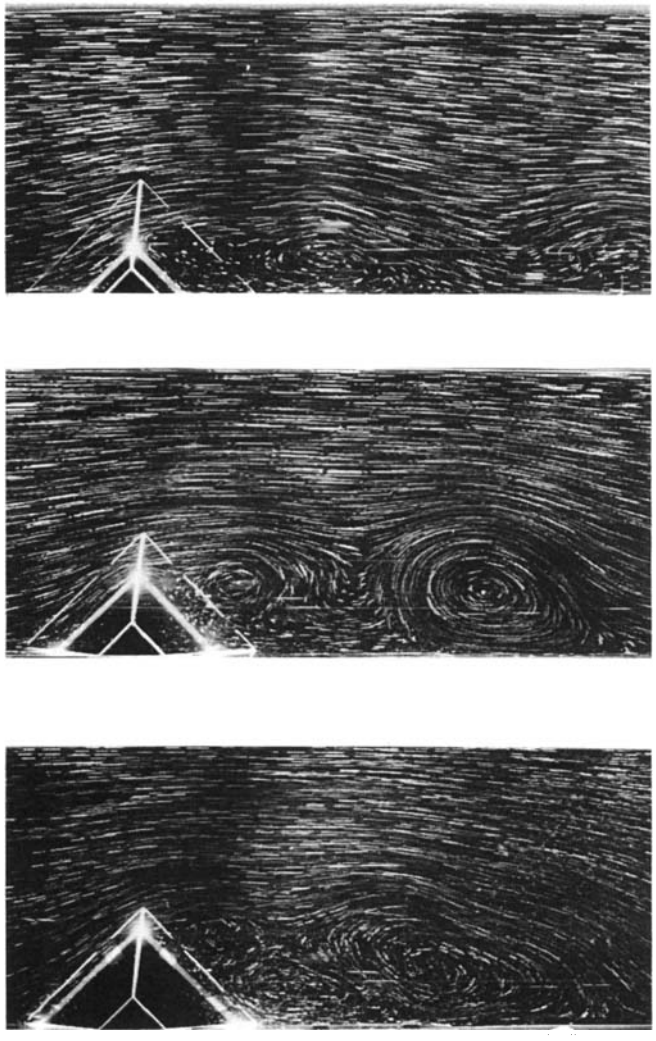

FIGURE 5. Vertical structure for anticyclonic-eddy-shedding regime; $Ro = 0.13$, $S = 6.48$. $E = 6.2 \times 10^{-4}$ ($Re = 550$); (a) $\tau^* = 9.9$, $z^* = 0.75$, (b) 9.5, 0.50 and (c) 8.9, 0.25.

For somewhat larger S and for a range of Ro, with the obstacle still on the right, an attached anticyclonic eddy is established. Figure 3 depicts a time sequence of flow patterns for the middle level for this characteristic flow which we term an 'attached anticyclonic eddy' regime. Note that in the example given the anticyclone develops quite slowly with full development requiring of the order of ten advective timescales. Figure 3(c) is the last photograph in the obstacle traverse and represents what is believed to be an approximately steady-state pattern.

For homogeneous flows one might expect the attached lee eddy to spin down by Ekman suction for the Ro and E values used in the experiments of figure 3. Rapid spindown in the middle levels is not occurring, however, evidently because stratification effects are limiting the influence of Ekman suction to the regions in the immediate vicinity of the upper and lower bounding surfaces. It should be pointed out that the Ekman layers themselves have the same structure as that for homo-

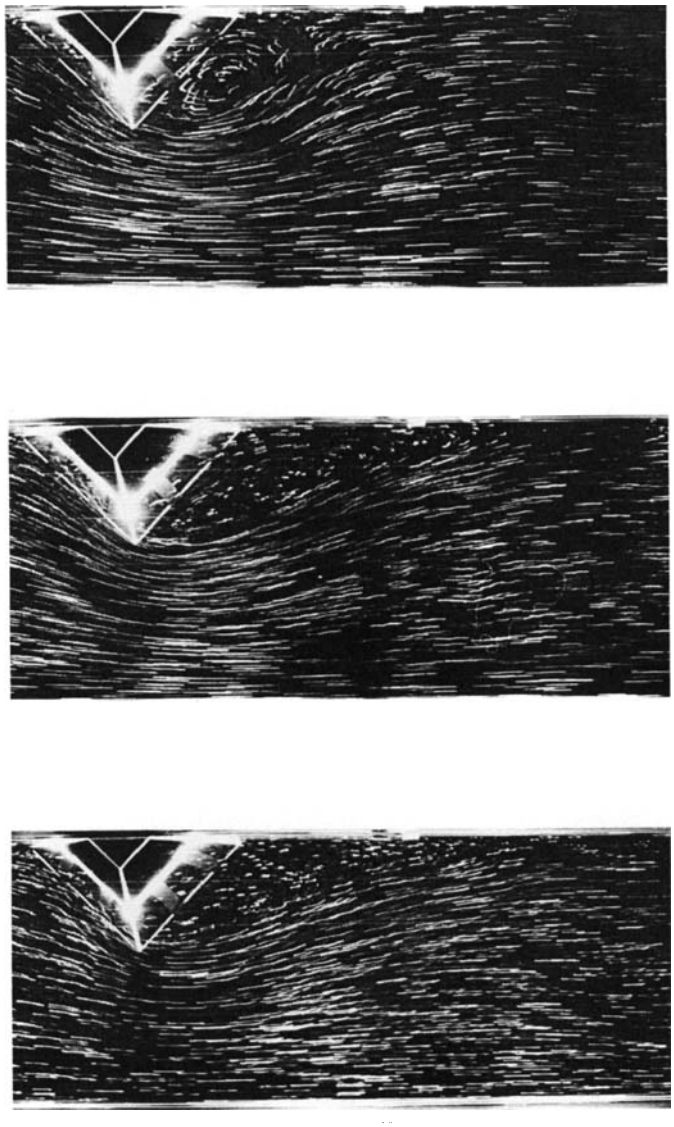

FIGURE 6. Temporal development of attached-cyclonic-eddy regime; $Ro = 0.023$, $S = 0.26$, $E = 1.6 \times 10^{-4}$ ($Re = 390$), $z^* = 0.50$; (*a*) $\tau^* = 2.1$, (*b*) 5.5 and (*c*) 9.1.

geneous systems because $E \ll Ro/S$; see the analysis in Pedlosky (1979, pp. 338–339). The response in the interior regions to this so-called Ekman suction, however, is far more complicated for the case of stratified fluids. For the present geometry the eddies themselves have a complex three-dimensional structure with the theoretical investigation of the generation and maintenance (decay) of eddies such as discussed herein requiring a fully three-dimensional nonlinear analysis.

Continuing with the right-side-mounted obstacle but at still larger S and for a range of Ro, a well-defined anticyclonic eddy is established in the obstacle lee at characteristic dimensionless times, $\tau^* \approx 1$. A time sequence of this larger S case for the middle level is given in figure 4(*a–c*). Note that the starting eddy is subsequently shed and replaced by a weaker second anticyclone. Figure 4(*c*) represents the last

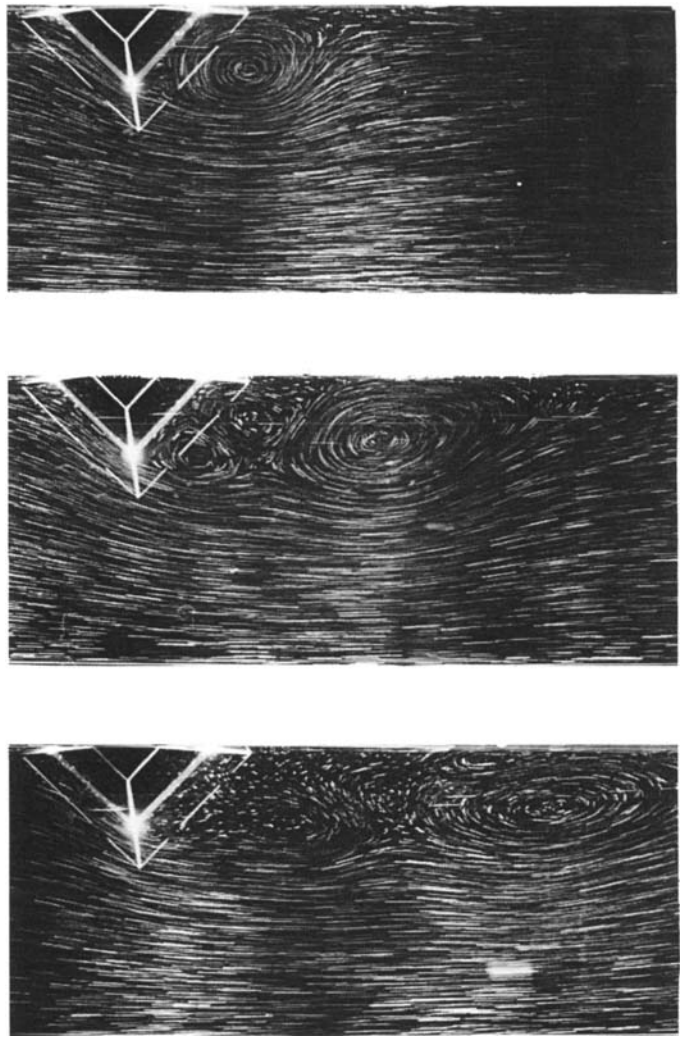

FIGURE 7. Temporal development of cyclonic-eddy-shedding regime; $Ro = 0.13$, $S = 6.48$, $E = 6.2 \times 10^{-4}$ ($Re = 560$), $z^* = 0.50$; (a) $\tau^* = 2.1$, (b) 6.3 and (c) 10.6.

observation in the obstacle traverse so that the long-time behaviour for this characteristic flow could not be observed with the present apparatus. We term this regime as 'anticyclonic eddy shedding'.

Figure 5(*a–c*) depicts observations at various levels near the end of the obstacle traverse for the experiment shown in figure 4. Figure 5(*a*) shows that the wake is significantly narrower in the upper portion of flow compared with the lower levels as exemplified by figure 5(*b*,*c*). This is due to the flow field being largely horizontal at all levels and to the relatively small characteristic horizontal scale of the topography in the upper levels of the fluid. Note also that the eddy patterns in the mid-level (figure 5*b*) seem stronger (i.e. higher relative vorticity) and more well defined than that in the lower level (figure 5*c*). This is due to the rapid spindown of the eddies in the lower level as discussed above.

The flow patterns for left-side obstacles were dramatically different, especially at

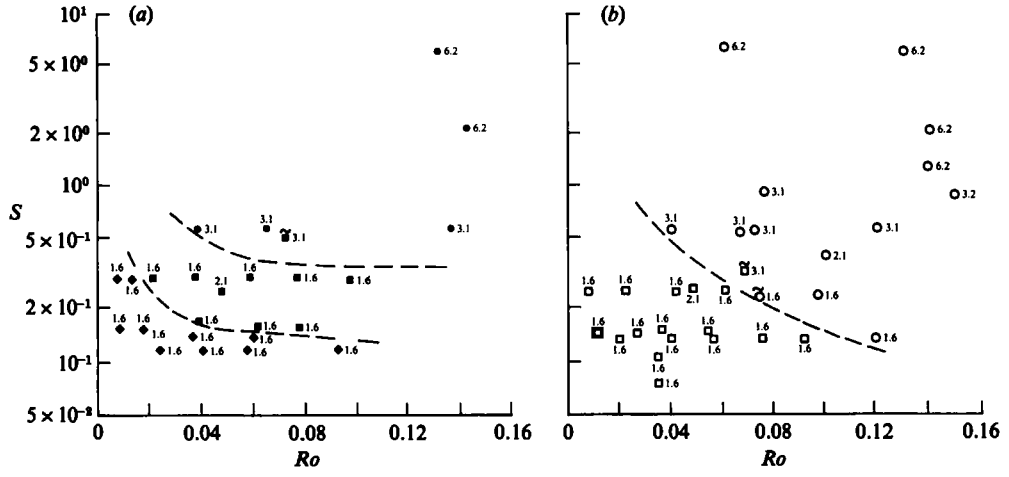

FIGURE 8. Flow-regime diagrams of Burger against Rossby number for (*a*) right-side and (*b*) left-side topography. The numbers in the vicinity of the symbols indicate the Ekman number $\times 10^4$ and the tildes represent runs of uncertain classification. The dashed lines are the approximate divisions between the various flow regimes. The regimes are fully attached anticyclonic (◆), attached anticyclone (■), anticyclonic-eddy shedding (●), attached cyclone (□) and cyclonic-eddy shedding (○).

the smaller values of S. The first observation was that for the smallest Burger and Rossby numbers considered, no fully attached regime, such as that noted for the right-mounted obstacle, was obtained. For sufficiently small S and Ro, a lee cyclonic eddy was established in a timescale, $\tau^* \approx 1$. That eddy was subsequently observed to spin down leaving a wake in which the characteristic motions were exceedingly small. Figure 6(*a–c*) depicts a time sequence of such a flow pattern for the middle level; we term this regime an 'attached cyclonic eddy'. Note that for the attached-anticyclonic-eddy regime (e.g. figure 3), the lee eddy is formed slowly (i.e. on the order of many advective timescales) and then retains its intensity, while for similar dimensionless parameters for the left side the lee eddy is quickly formed, but subsequently spins down. Observations at different levels for the attached-cyclonic-eddy regime indicate that the size of the quiescent wake region decreases with height, as might be expected.

At larger values of S and Ro for the left-side obstacle (see the regime diagram in figure 8), a lee cyclone is established in a characteristic time, $\tau^* \approx 1$. This cyclone sheds and is subsequently advected downstream and replaced by a second, but weaker, cyclone. An example of this process is given by the time sequence of flow patterns at mid-level in figure 7(*a–c*).

By comparing figures 4(*a–c*) and 7(*a–c*), one notes that the right- and left-side obstacles, respectively, have similar characteristic flow patterns; i.e. they are essentially 'mirror images'. We term the left-side flow as depicted in figure 7(*a–c*), 'cyclonic eddy shedding' and consider this to be the counterpart of the anticyclonic-eddy-shedding regime for the right-side obstacle. It is noted that for the eddy-shedding cases, exemplified by the experiments of figures 4 and 7, the tow tank was not of sufficient length to enable the observation of the eddy-shedding period and hence the measurement of a Strouhal number.

Flow-regime diagrams of Burger against Rossby number indicating the regions in parameter space for which the above characteristic flows are observed for the right

and left side are given in figure 8(*a*, *b*), respectively. Note that the Ekman-number values are given for each data point and that experiments of uncertain designation are indicated by a tilde above the symbol. We shall now consider some quantitative measures of the observations.

4. Experimental results – quantitative

The objectives in developing quantitative measures of the observations were two-fold. The first was to more clearly define some of the observations noted in the previous section with the possibility of comparison with similar flow characteristics in the oceans or atmosphere. The second was to record a set of observational data that could be used for comparison purposes by analytical or numerical modellers interested in the present physical system. The observables considered both important and measurable with some degree of accuracy were the location of the eddy centres, the streamwise extent of the eddies and a mean vorticity of the eddy cores. These parameters were generally measured as functions of the dimensionless time $\tau^* = Ut/D$, and the dynamical parameters Ro, S and E.

The analysis for each particle-streak photograph was carried out in the following way. The streamwise location x_c of the centre of each eddy was first determined, giving the dimensionless location $x_c^* = x_c/D$; see figure 1. This measure, of course, could not be made for cases of fully attached flow (e.g. figure 2), for the small-time wake of the attached-anticyclonic-eddy regime (e.g. figure 3*a*, *b*) or for the long-time wake for the attached-cyclone regime (e.g. figure 6*c*).

An estimate of the streamwise extent of the separated region was obtained by first locating the approximate streamline dividing the separated region from the external flow; see figure 1. This streamline was then followed until its distance from the wall (i.e. y-direction) was $\frac{1}{5}D$. The dimensionless, streamwise distance $x_e^* = x_e/D$ of this point from the centre of the obstacle (i.e. $x = 0$) was then determined; see figure 1.

The final observable was the dimensionless mean vorticity $\zeta^* = D\zeta/U$ of the eddy cores, where ζ is the dimensional vorticity. To determine ζ, a circle of diameter $d = \frac{1}{2}D$ was drawn around the eddy centre; see figure 1. The circulation Γ was then determined by measuring the tangential velocity components at eight approximately equally spaced intervals around the circle; thus $\Gamma = \pi d\bar{v}_t$, where $\bar{v}_t$ is the average tangential velocity. Stokes theorem was then used to relate the average vorticity within the circle to the circulation; i.e. $\zeta = 4\Gamma/\pi d^2$.

Vorticity is, of course, a troublesome quantity to measure in experiments such as those being considered. The first question arising for the above method concerns the typical core size of the eddies being measured. For example, if $\frac{1}{2}d$ extends substantially beyond the outer edge of the core, the technique will seriously underestimate ζ. To examine this question the dimensionless velocity profiles, u_t/U against r/D, along the major and minor axis of the eddies depicted in figures 3(*c*), 4(*b*) and 7(*b*), were obtained; here r represents the distance from the eddy centre and the results are given, respectively, in figure 9(*a–c*). The value of $r/D = 0.25$ at which the circulation is measured is indicated in each plot of figure 9. Note that the radius of the measurement circle is always less than the distance of the maximum velocity from the eddy centre; we thus conclude that reasonable estimates of the core vorticity are obtained by this method.

In order to obtain an estimate of the statistical limits of error for each of the above observables, a series of 11 independent experiments was conducted under the same experimental conditions. In these experiments the dimensional parameters were fixed

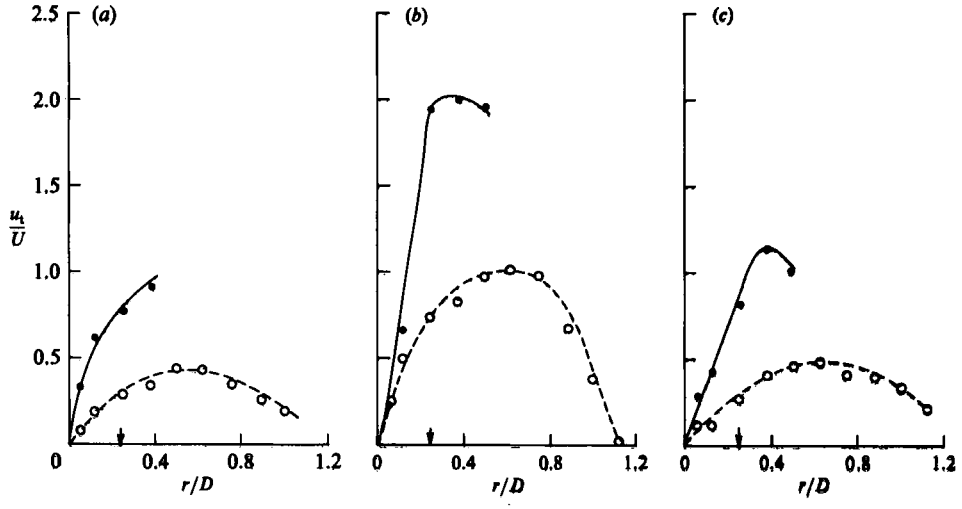

FIGURE 9. Dimensionless velocity profiles across major (--○--) and minor (—●—) axes of the lee eddies depicted in (*a*) figure 3(*c*), (*b*) figure 4(*b*) and (*c*) figure 7(*b*). Small arrows at $r/D = 0.25$ indicate the radius at which circulation is calculated (see text).

τ^*	$\bar{x}_c^*$	$\frac{\delta x_c^*}{\bar{x}_c^*}$ (%)	$\bar{x}_e^*$	$\frac{\delta x_e^*}{\bar{x}_e^*}$ (%)	$\bar{\delta}^*$	$\frac{\delta \zeta^*}{\bar{\zeta}^*}$ (%)
2.2	1.2	5	2.2	5	7.5	8
4.4	1.7	9	3.0	4	6.0	11
7.4	2.2	11	4.4	3	4.4	9

TABLE 2. Error analysis (for description see text)

at the following values: $U = 0.48$ cm s^{-1}, $\omega = 0.25$ s^{-1}, $N = 0.76$ s^{-1}, $\nu = 0.01$ cm^2 s^{-1} and a left-side-obstacle location was considered. For each experimental run particle-streak photographs were taken at $t = 60$, 120 and 200 s (i.e. $\tau^* = 2.2$, 4.4 and 7.4). Taking 3 s.d./$n^{\frac{1}{2}}$ as the statistical limit of error δ, where s.d. is the standard deviation, table 2 provides the results of the error analysis. We conclude that the statistical limits of error for x_c^*, x_e^* and ζ^* are roughly 10%, 5% and 10%, respectively. Error bars of this magnitude can be assumed in the following observations.

4.1. *Lee-eddy location and extent*

Figure 10(*a*, *b*) shows the dimensionless streamwise location x_c^* against the dimensionless time τ^* for cases of eddy shedding at a fixed Burger number $S = 0.57$ and for the Rossby numbers $Ro = 0.40$ and 0.068, respectively. The right-side experiments are indicated by solid symbols and the left by open symbols, while the observation level is indicated by the different symbol shapes (see figure captions). Note that the time dependence of x_c^* for the right side is approximately the same as that for the left but with larger scatter for the former. This larger variation of the eddy structure on the right was a general observation for all experiments conducted in the eddy-shedding regimes. The data also show no systematic variation of x_c^* with observation level so that, within the accuracy of the measurements, the axes of the shed eddies are vertical.

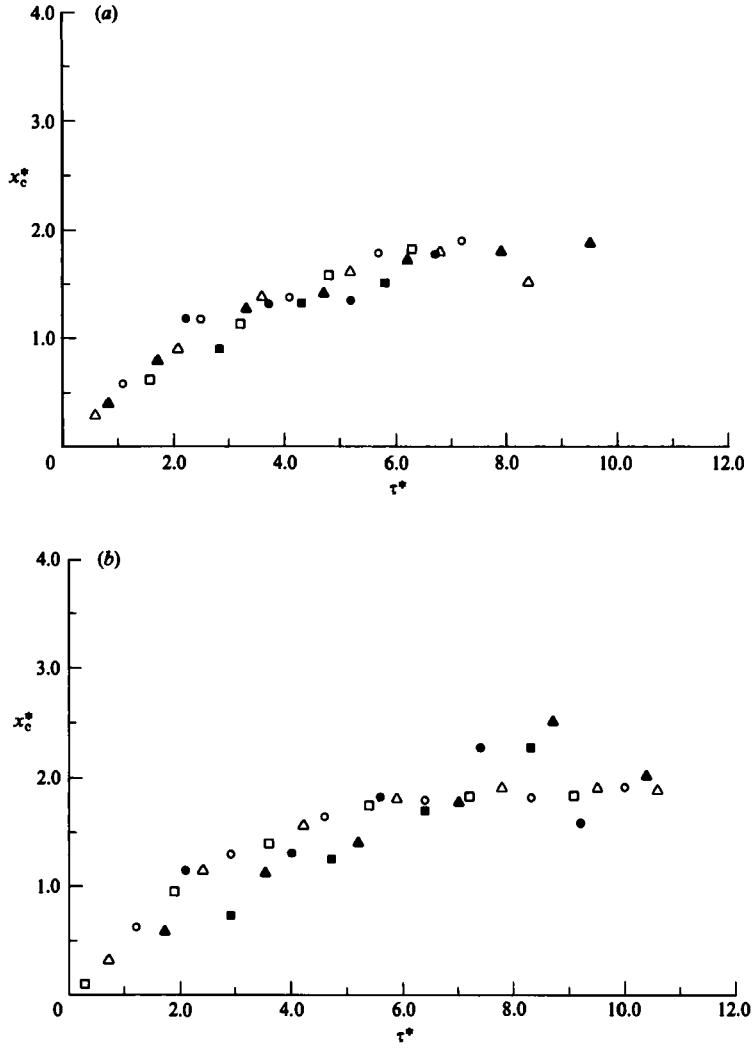

FIGURE 10. Dimensionless streamwise location of eddy centre x_c^*, against τ^* for $S = 0.57$, $E = 3.1 \times 10^{-4}$; (*a*) $Ro = 0.40$, $Re = 340$ and (*b*) 0.68, 570. The observation levels z^* are given by 0.25 (●, ○), 0.50 (▲, △) and 0.75 (■, □), where solid symbols are anticyclones and open symbols are cyclones.

Note that at large τ^* the eddy centres of figures 10(*a*, *b*) asymptotically approach a fixed downstream distance $x_c^* \sim 2$ from the cape; the eddies are observed to decay but to retain their identity over the duration of the experiment. As can be noted on figure 8, the experiments of figure 10(*a*, *b*) are near the attached-eddy regime and the detached eddies are thus not vigorously advected downstream. This is contrasted by those experiments at larger S in figure 4 (right side) and figure 7 (left side) for which the shed eddies continue to advect downstream (and in the process decay by Ekman suction).

Figure 11(*a*, *b*) gives the streamwise extent x_e^* against τ^* for the attached-eddy regime for a range of Rossby numbers at approximately fixed $S = 0.31$ (right side) and 0.26 (left side), respectively. From figure 11(*a*) we note that for the right side

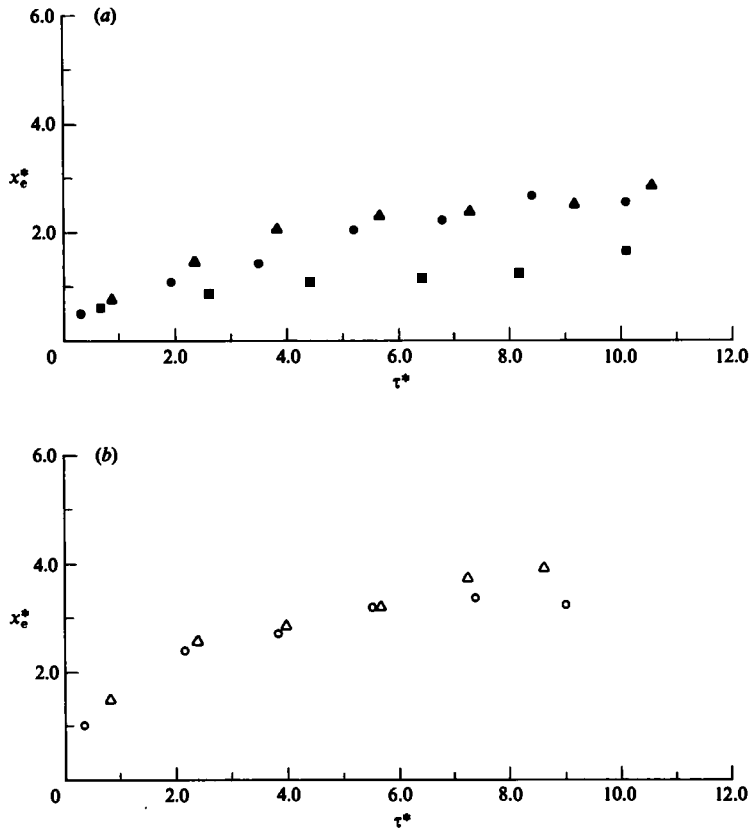

FIGURE 11. Dimensionless eddy length x_e^* against τ^* for various Ro for (*a*) attached-anticyclonic-eddy regime with $S \approx 0.31$, $E \approx 1.6 \times 10^{-4}$ and (*b*) attached-cyclonic-eddy regime with $S \approx 0.26$, $E \approx 1.6 \times 10^{-4}$. (*a*) $Ro = 0.021$, $Re = 360$ (●); 0.058, 990 (▲); 0.097, 1640 (■); and (*b*) $Ro = 0.023$, $Re = 390$ (○); 0.061, 1030 (△).

the smallest x_e^* (i.e. the smallest wake region) occurs for the largest Rossby number with x_e^* for the two smallest Ro asymptotically approaching the same $x_e^* \sim 2.7$. While the Burger numbers in the experiments of figure 11 (*a*, *b*) are slightly different, we note the tendency for larger lee eddies for the left side in the attached-eddy regime for otherwise fixed parameters; i.e. compare the $Ro = 0.021$ and 0.023 and the $Ro = 0.058$ and 0.061 runs of figure 11 (*a*, *b*) respectively.

The first objective of the vorticity measurements was to obtain a measure of the core vorticity of starting eddies in the eddy-shedding regimes as functions of time and elevation for the right and left sides, respectively, for fixed S and Ro. Figures 12 (*a*) (right) and 12 (*b*) (left) are single experiments in which the observation level was being changed during the course of the experimental runs; note the staggering of the experimental points with τ^*. Note that the maximum vorticity at all levels is attained more rapidly for the left (i.e. cyclonic) side and that the maximum ζ^* is about the same at corresponding levels for both the anticyclones and cyclones. The eddies are noted to decay by Ekman suction for both sides with the decay being more rapid for the cyclones at all levels.

Both anticyclones and cyclones indicate a stronger core vorticity in the lower levels at small τ^*. This should be expected because the characteristic horizontal dimension

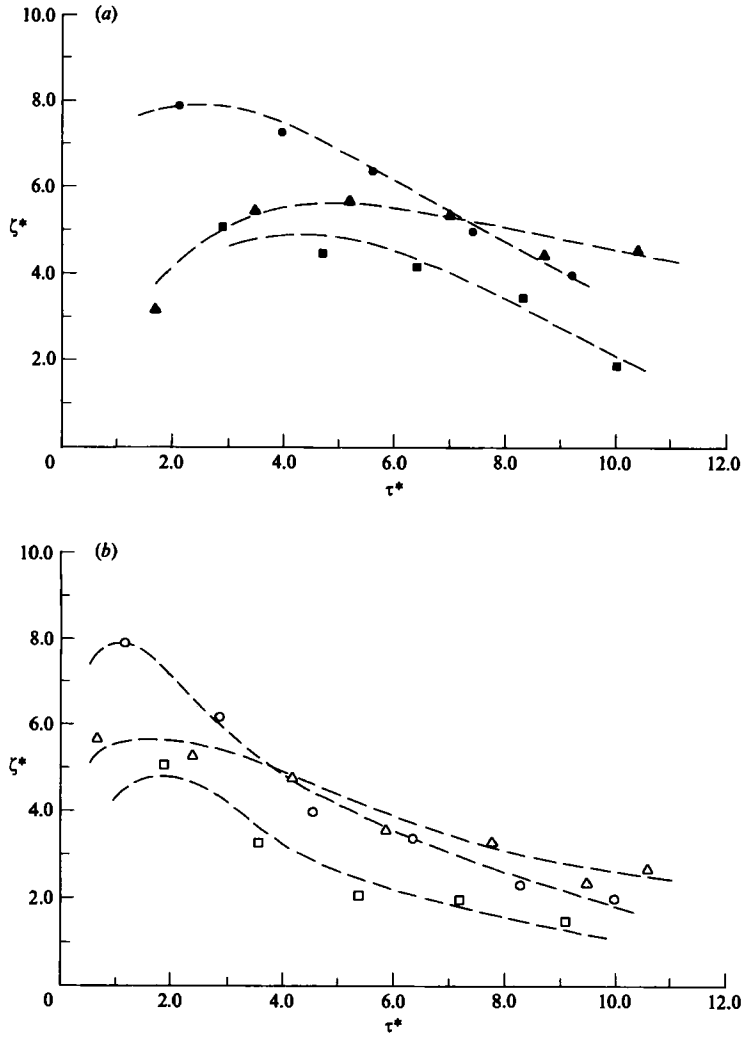

FIGURE 12. Dimensionless vorticity ζ^* of a starting eddy against τ^* for various elevations z^* for (*a*) anticyclonic ($Ro = 0.065$, $Re = 550$) and (*b*) cyclonic ($Ro = 0.068$, $Re = 570$) eddy-shedding regimes; $S = 0.57$ and $E = 3.1 \times 10^{-4}$. (*a*) $z^* = 0.25$ (●); 0.50 (▲); 0.75 (■); and (*b*) 0.25 (○); 0.50 (△); 0.75 (□). The dashed lines represent the approximate fit to the data.

of the topography is largest there and thus, combined with the tendency for both rotation and stratification to inhibit vertical motion, generates stronger horizontal shear. The decay patterns at the various observation levels are seen to differ substantially. As also should be expected the decay by Ekman suction is strongest near the bottom where the core vorticity is largest (at small τ^*) and where the suction is most effective. This leads to stronger vorticities in the middle level (i.e. compared with the upper and lower levels) at large τ^* for both anticyclones and cyclones; see figure 12(*a*, *b*).

Figure 13(*a*, *b*) depicts measurements of the core vorticity in the middle level against time for the anticyclonic- and cyclonic- eddy-shedding regimes, respectively, for approximately fixed S and various Ro. We note first that the dimensionless vorticity for the starting anticyclone is largest at small τ^* for the smallest Rossby

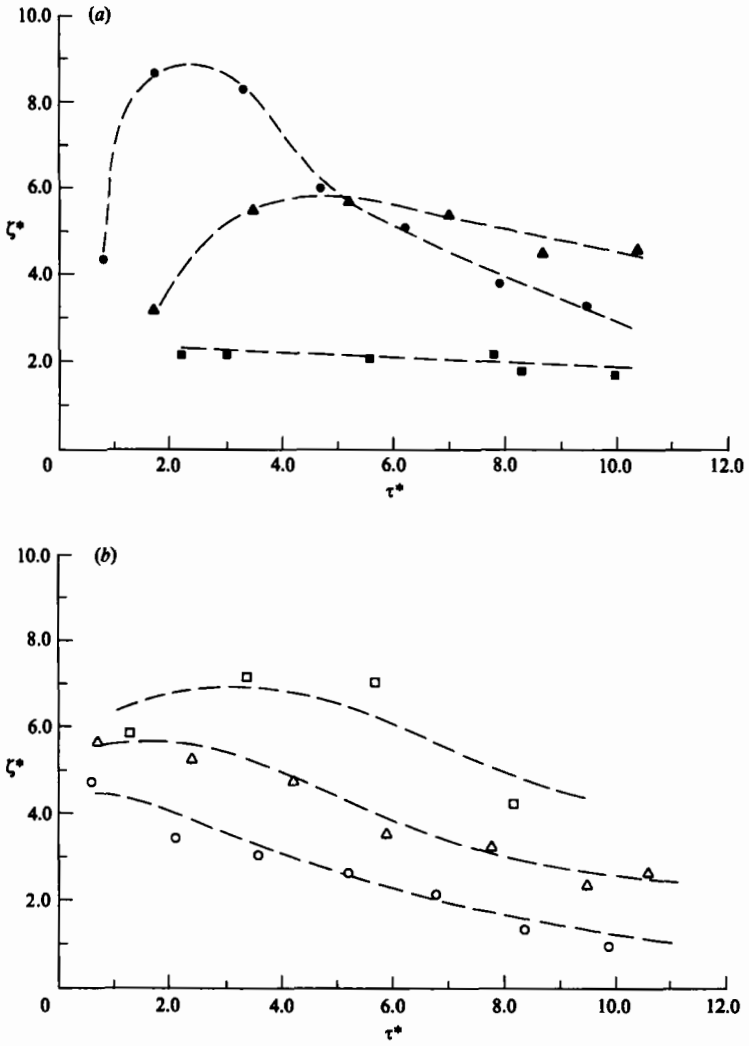

FIGURE 13. Dimensionless vorticity ζ^* of a starting eddy against τ^* for various Ro, Re for (a) anticyclonic- and (b) cyclonic-eddy-shedding regimes; $S = 0.57$, $E = 3.1 \times 10^{-4}$ and $z^* = 0.50$. (a) $Ro = 0.038$, $Re = 320$ (●); 0.065, 550 (▲); 0.13, 1080 (■); and (b) 0.040, 340 (○); 0.068, 570 (△); 0.12, 1050 (□). The dashed lines represent the approximate fit to the data.

number (i.e. $Ro \approx 0.038$) and that this vorticity then decays rapidly with time, being less than the intermediate Ro (i.e. $Ro \approx 0.065$) at large τ^*. The vorticity for the largest Ro (i.e. $Ro \approx 0.13$) is small and is almost independent of τ^*. The behaviour of the starting cyclone, as depicted in figure 13(b), is quite different. Here the cyclone is weak, for all τ^* for the smallest Ro; the decay with τ^* is evident for all cases.

The next experiments addressed the question of the strength of the vorticity for examples of the attached anticyclone and cyclone regimes. We recall that for the right side, anticyclones developed slowly in terms of τ^* but at the end of the traverse were of substantial strength (see figure 3). For the left side, on the other hand, cyclones developed quickly but were then spun down at large τ^*. This is clearly evident in the data. Figure 14(a) is a plot of all of the experiments conducted for the anticyclonic side for $S \approx 0.31$ and for a range of Ro given by $0.021 \leqslant Ro \leqslant 0.097$ (see figure 8).

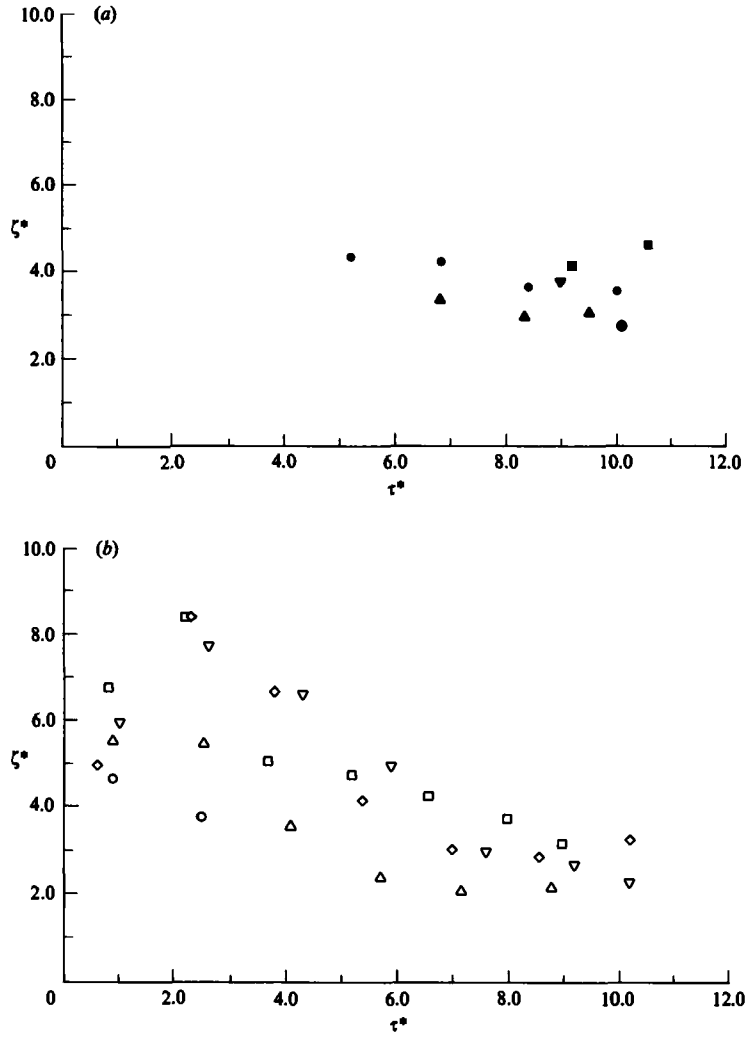

FIGURE 14. Dimensionless vorticity ζ^* of a lee eddy against τ^* for various Ro, Re for attached (*a*) anticyclonic- ($S = 0.31$) and (*b*) cyclonic- ($S = 0.14$) eddy regimes; $E = 1.6 \times 10^{-4}$ and $z^* = 0.50$. (*a*) $Ro = 0.021$, $Re = 360$ (●); 0.038, 650 (△); 0.058, 990 (■); 0.078, 1310 (▼); 0.097, 1640 (◆); and (*b*) 0.021, 350 (○); 0.041, 690 (△); 0.056, 950 (□); 0.078, 1310 (▽); 0.093, 1570 (△).

We note first that for smaller Ro at $S \approx 0.31$ ($Ro = 0.007$, 0.014) the flow is fully attached, so that no eddy-core vorticity measurements could be made. We also note, in consonance with the observations of the slow development of anticyclones, that no measurements are available at small τ^* for all Ro investigated. As the various anticyclones develop, we note that $\zeta^* \approx 4$ with there being insufficient data to note any particular trend with Ro. The data for the cyclonic side, as given in figure 14 (*b*), indicates a development of a maximum core vorticity for all Ro (*i.e.* $0.021 \leqslant Ro \leqslant 0.093$) on the order of one to two advective timescales with a subsequent decay in vortex strength for all Ro considered. For the smallest $Ro = 0.021$ the eddy has decayed to such an extent that ζ^* cannot be ascertained after $\tau^* \approx 9$. The decay of ζ^* for the other Rossby-number runs is approximately the same

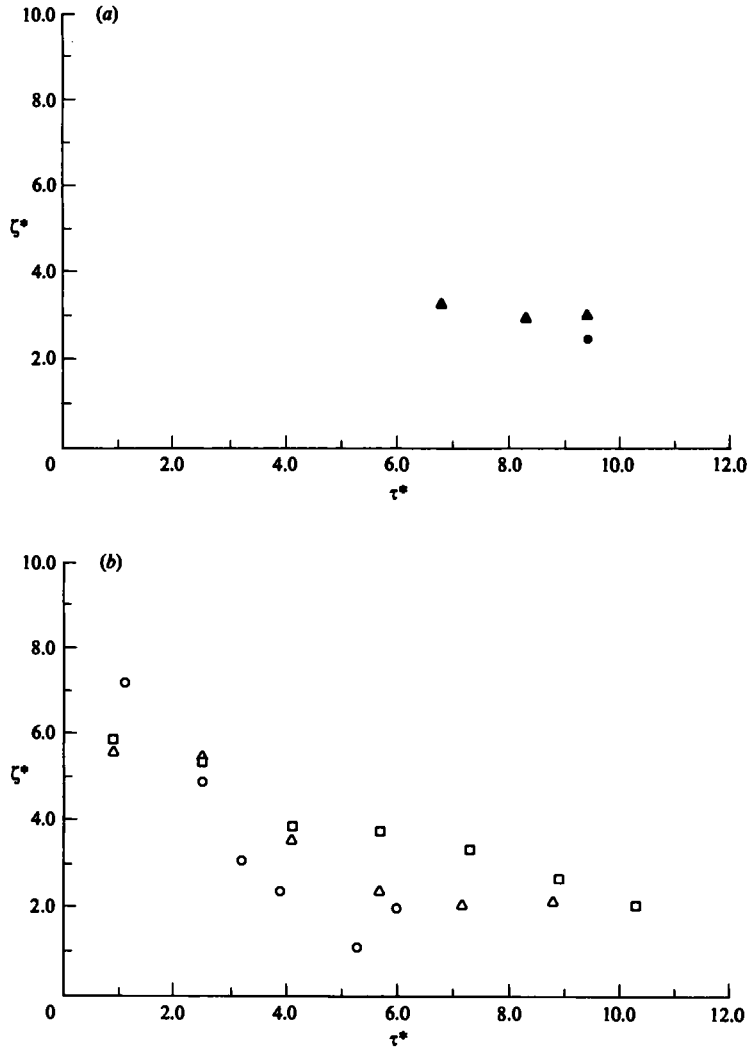

FIGURE 15. Dimensionless vorticity ζ^* of a lee eddy against τ^* for various S for attached (a) anticyclonic- ($S = 0.15$ (●); 0.31 (▲)) and (b) cyclonic- ($S = 0.075$ (○); 0.14 (△); 0.26 (□)) eddy regimes; $Ro \approx 0.04$, $E = 1.6 \times 10^{-4}$ ($Re \approx 650$) and $z^* = 0.50$.

after $\tau^* \approx 4$ and while the eddies are weak at large τ^* for those cases they are still distinguishable and a ζ^* measurement can be made. Figure 14(a, b) gives some quantitative measure of the differences between the attached anticyclone and cyclone patterns demonstrated qualitatively in figures 3 and 6, respectively.

Figure 15(a, b) depicts the variations of ζ^* against τ^* for right- and left-side topographies, respectively, for approximately fixed $Ro \approx 0.04$ and for a range of S for experiments in which the lee eddy is attached to the obstacle. For the anticyclonic side, figure 8(a) shows that for sufficiently small S (i.e. $S \leqslant 0.15$) the flow is fully attached and no ζ^* can be measured. For the larger S experiments we note that the lee eddy attains a core vorticity $\zeta^* \approx 3$ and that the time for development tends to decrease with increasing S.

Figure 15(b) shows the generally more rapid decay of vorticity with τ^* for smaller

S. For the lowest $S = 0.075$, for example, the eddy becomes essentially indistinguishable at $\tau^* \approx 6$. A decreased stratification level, as produced by smaller S, leads to more rapid decay of the lee eddies by Ekman suction.

5. Summary and concluding remarks

The flow of a linearly stratified, rotating fluid past capes with sloping sides mounted on either the left or right side of a rectangular channel has been investigated. For a range of Rossby numbers Ro and for experiments with increasing Burger numbers S, for the obstacle on the right one notes the following sequence of flow patterns:

(i) At sufficiently small S the flow is fully attached with the streamlines following the topography at all levels.

(ii) At intermediate S a lee anticyclone having a characteristic dimension of the order of the obstacle width develops during a period of the order of ten advective timescales.

(iii) At larger S the starting lee anticyclone sheds and is succeeded by a weaker anticyclone.

Similar observations for the left side demonstrate that:

(i) Flow separation in the lee occurs for all S investigated. For the smallest S experiments a lee cyclone forms during a period of the order of one advective timescale. This eddy, however, quickly spins down leaving a relatively quiescent region in the lee of the cape.

(ii) At sufficiently large S the starting lee cyclone is shed and is succeeded by a weaker cyclone.

Quantitative measures of the location of the eddy centres, the streamwise extent of the lee eddies and the mean vorticity of the eddy cores, as functions of the dimensionless time and the various system parameters have been presented. It is shown for example that near the cape (i.e. at small τ^*) the dimensionless vorticity is largest in the lowest layers of the fluid, smallest at the highest levels and intermediate in the middle levels. As the shed eddies advect downstream the vorticity in the middle levels spins down by Ekman suction more slowly than that in the lower levels leading, in fact, to the situation in which the vorticity in the middle levels exceeds that in the lowest layers. Elliot & Sanford (1986*a*, *b*) have recently discussed the characteristics of what they term a subthermocline lens found in the open ocean. In effect this feature is an eddy having a strong signature in mid-levels and relatively weak signatures in the upper and lower levels. One possible source for such structures could be the shedding of vortices from submarine topographic features with the subsequent strong decay of the structure in the lower levels as observed in the present experiments.

One reviewer noted that capes are typically embedded in shelf-slope regions and, as such, the present model may have limited oceanographic implications. The reviewer pointed out that the bottom slopes are generally less than the cape slopes but can be comparable in value. These bottom slopes provide an ambient potential-vorticity gradient which would tend to produce horizontal lee waves if the approach current has the coastline to the left. For the coastline on its right the reviewer suggested that the approach current would experience a strong decay in the lee. It is, of course, true that the physical system considered above is one of very simplified geometry. The wake would clearly be different, both qualitatively and quantitatively for the flow past capes that are superimposed on long shallow bottom slopes. This would be a fruitful area, for further investigation, but will not be considered further

in the present study. The situation referred to is similar to that considered by one of the present authors in a recent study on the homogeneous flow past a right circular cylinder on a β-plane (simulated by considering the flow through a sloping channel); see Boyer & Davies (1982). That study indicated the dramatic differences that can occur for eastward (corresponding to a sloping bottom with the coastline on the left), westward (coastline on the right) and f-plane flow (that considered herein).

The authors acknowledge, with thanks, the support of the US National Science Foundation under grants ATM-8218488 and ATM-8514781. Appreciation is also extended to the Institute of Atmospheric Physics, Academia Sinica, for the leave of absence granted to Mrs Lijun Tao for her research work at the University of Wyoming.

REFERENCES

BAINES, P. G. & DAVIES, P. A. 1980 Laboratory studies of topographic effects in rotating and/or stratified fluids. In *Orographic Effects in Planetary Flows* (ed. R. Hide & P. W. White), pp. 233–229. GARP Publications Series No. 23, World Meteorological Organization, Geneva.

BOYER, D. & BIOLLEY, F. 1986 Linearly stratified rotating flow over long ridges in a channel. *Phil. Trans. R. Soc. Lond.* A **318**, 411–438.

BOYER, D. & KMETZ, M. L. 1983 Vortex shedding in rotating flows. *J. Geophys. Astrophys. Fluid Dyn.* **26**, 51–83.

BOYER, D. L. & DAVIES, P. A. 1982 Flow past a circular cylinder on a β-plane. *Phil. Trans. R. Soc. Lond.* A **306**, 533–556.

BOYER, D. L., DAVIES, P. A., HOLLAND, W. R., BIOLLEY, F. & HONJI, H. 1987 Stratified rotating flow over and around isolated three-dimensional topography. *Phil. Trans. R. Soc. Lond.* (in press).

DAVIES, P. A. 1972 Experiments on Taylor columns in rotating stratified fluids. *J. Fluid Mech.* **54**, 691–717.

ELLIOT, B. A. & SANFORD, T. B. 1986*a* The subthermocline lens D1. Part 1: Description of water properties and velocity profiles. *J. Phys. Oceanogr.* **16**, 532–548.

ELLIOT, B. A. & SANFORD, T. B. 1986*b* The subthermocline lens D1. Part 2: Kinematics and dynamics. *J. Phys. Oceanogr.* **16**, 549–561.

GRIFFITHS, R. W. & LINDEN, P. F. 1983 The influence of a sidewall on rotating flow over bottom topography. *Geophys. Astrophys. Fluid Dyn.* **27**, 1–33.

OSTER, G. 1965 Density gradients. *Scient. Am.* **213**, 70–76.

PEDLOSKY, J. 1979 *Geophysical Fluid Dynamics*. Springer.